DEPENDENCE OF HYDROGEN EMBRITTLEMENT ON HYDROGEN IN THE SURFACE LAYER IN TYPE 304 STAINLESS STEEL

Zhang, L. [1], Li, Z.Y. [2], Zheng, J.Y. [2*], Zhao, Y.Z [2], Xu, P. [2], Zhou, C.L. [2]

[1] Institute of Materials and Surface Engineering, Zhejiang University of Technology, Hangzhou 310014, China, zhlin@zjut.edu.cn

[2] Institute of Process Equipment, Zhejiang University, Hangzhou 310027, China, jyzh@zju.edu.cn (Zheng, J.Y., corresponding author)

ABSTRACT

Hydrogen embrittlement (HE) together with the hydrogen transport behavior in hydrogen-charged type 304 stainless steel was investigated by combined tension and outgassing experiments. The hydrogen release rate and HE of hydrogen-charged 304 specimens increase with increasing the hydrogen pressure for hydrogen-charging (or hydrogen content) and almost no HE is observed below the hydrogen content of 8.5 mass ppm. Baking at 433 K for 48 hours can eliminate HE of the hydrogen-charged 304 specimen, while removing the surface layer will restore HE, which indicates that hydrogen in the surface layer plays the primary role in HE. Scanning electron microscopy (SEM) and scanning tunnel microscopy (STM) observations show that particles attributed to the strain-induced α' martensite formation break away from the matrix and the small holes form during deformation in the hydrogen-charged 304 specimen. With increasing strain, the connection among small holes along {111} slip planes of austenite will cause crack initiation on the surface, and then the hydrogen induced crack propagates from the surface to interior. This result will be favorable to develop the technology for HE prevention in hydrogen utilization.

1. INTRODUCCTION

Hydrogen has been expected to be used as a source of clean energy, particularly as the fuel for fuel cell systems; thus hydrogen storage and transportation have become a key technology for fuel cell systems. Since hydrogen storage using high pressure hydrogen gas is an important method for hydrogen supply, the development of hydrogen storage systems has been conducted throughout the world [1]. Austenitic stainless steels are commonly used for the components of fuel cell systems, such as liners of high pressure vessels of 70 MPa class, piping, valves, springs, etc [2]. These components are directly exposed to hydrogen gas environment, subjected to concurrent hydrogen uptake with mechanical loading, thus hydrogen embrittlement (HE) of the metal, particularly in a hydrogen atmosphere (hydrogen gas embrittlement, HGE), occurs[3, 4]. Hydrogen is also absorbed by the metal, thus HE of the metal by internal hydrogen (internal reversible hydrogen embrittlement, IRHE) also occurs[5, 6]. The prevention of both HGE and IRHE is critical for the safe use of hydrogen transport and distribution.

In general, there is a threshold hydrogen concentration below which embrittlement does not occur. Singh et al. [7] found that no slow crack growth (SCG) occurred in stainless steels having hydrogen contents less than a threshold value, and the hydrogen contents in the various steels were changeable according to their chemical compositions. However, it has been found recently that the hydrogen at a level of 2 to approximately 3 wppm definitely increases fatigue crack growth rates in austenitic stainless steels, when the loading frequency is reduced to 0.0015 Hz [8]. Most research works focused on the total hydrogen content in the bulk specimen, while the hydrogen contents of the surface layer and interior are different due to hydrogen entry and outgassing. Till now, the dependence of HE on the hydrogen distribution is still ambiguous.

The rate control process of HGE may be the surface process, i.e., adsorption; that of IRHE is the diffusion. The basic process of cracking of HGE that hydrogen atoms diffuse to the sensitive zone with stress concentration and induce cracking is similar to that of IRHE [9]. Since the rate controlling

processes of HGE and IRHE are different, cracking occurs almost on the surface in HGE, while it occurs inside the metal in IRHE [10]. However, Buckley et al. [11] showed that the hydrogen induced crack (HIC) initiated at the free surface of hydrogen- charged metastable austenitic steels during deformation at room temperature. Therefore, one important characteristic of IRHE that has not been resolved is the location of crack initiation: at the surface or internally.

Deformation-induced hydrogen release (DIHR) from metals has been studied under various mechanical interactions because of its importance in the ultrahigh vacuum (UHV) technology [12, 13]. Donovan [14] first applied DIHR to investigate tritium transport by dislocations in metals and Shoda et al. [15] applied DIHR in high vacuum to characterize hydrogen transport by dislocations in metals. Recently, we found that DIHR provides a possibility to evaluate the hydrogen transport behavior in austenitic stainless steel during plastic deformation [16].

In this study, we investigated the hydrogen transport behavior together with HE in hydrogen-charged type 304 and 310S stainless steels during deformation by combined tension and outgassing experiments, and identified the crack initiation related with the hydrogen distribution (depth profile).

2. EXPERIMENTAL

A UHV system with a quadrupole mass spectrometer and a temperature controllable tensile unit was developed. A pressure increase against the basal pressure (below 1.5×10^{-11} Torr) by released gas during tensile testing was measured and the hydrogen release rate was derived from the hydrogen partial pressure [17]. Type 304 steel (8.11% Ni, 18.27% Cr, 1.02% Mn, 0.65% Si, 0.05% C) and type 310S steel (19.4% Ni, 24.6% Cr, 1.28% Mn, 0.05% C, 0.79% Si) were solution-annealed at 1393 K for 1 hour after rolling into plates. The specimens with a gauge size of $10\times5\times1$ mm^3 for tensile test were machined from the plate. The high-pressure hydrogen storage for fuel cell systems requires the pressure up to 70 MPa and the temperature from -40 to 85 ℃. According to the Sievert's law, the hydrogen solubility of austenitic steels in 70 MPa hydrogen at 85 ℃ is approximately 40 mass ppm, which is similar to the hydrogen solubility of austenitic steels in 30 MPa hydrogen at 200 ℃. In order to realize the accelerated failure analysis, we adopted the thermal hydrogen charging method. The specimens were electro-polished in a solution of 90% CH_3COOH and 10% $HClO_4$, and then thermally hydrogen-charged in 1.0, 1.5, 4.0 and 30.0 MPa hydrogen gas at 473 K for 250 hours, respectively. The total hydrogen concentration in the specimen was measured by LECO RHEN602 hydrogen determinator in which hydrogen is analysed by inert gas fusion thermal conductivity detection. Tensile tests were conducted with a strain rate of 1.7×10^{-4} s^{-1} at 295 ± 2 K after the pressure was stabilized in the UHV chamber. The surface topography of the specimen after deformation was analyzed by scanning electron microscopy (SEM) and scanning tunnel microscopy (STM).

3. RESULTS

Stress-strain, hydrogen release curves for as-received and hydrogen-charged 304 specimens during deformation are shown in Fig. 1. The stresses of 1.0 and 1.5 MPa hydrogen-charged and as-received specimens increase with strain, attain the ultimate tensile strength (UTS), decrease with further strain until fracture, while 4.0 and 30.0 MPa hydrogen-charged specimens fracture much earlier and show the obvious HE characteristic, as shown in Fig. 1(a). This indicates that the HE susceptibility increases with the hydrogen pressure for hydrogen-charging. When the hydrogen pressures are 1.0 and 1.5 MPa, the decreases in ductility are fairly small, and their fracture stresses are higher than that of the as-received specimen, which shows weak HE. It is noted that several small anomalous stress peaks occur on the strain-stress curve above 50% strain, which has been reported in our previous work [18]. The hydrogen release rate of the as-received specimen rapidly increases to a small sharp peak in elastic deformation, increases to a small broad peak in the initial plastic deformation, and then decreases with increasing strain until fracture, while the hydrogen release rates of hydrogen-charged specimens increase with strain after elastic deformation until fracture, as shown in Fig. 1(b). The

slopes of the hydrogen release rates increase with the hydrogen pressure for hydrogen-charging, which is caused by the gradient of hydrogen concentration near the specimen surface.

Hydrogen contents of as-received and hydrogen-charged 304 specimens are shown in Fig. 2. The hydrogen content is also calculated according to the Sievert's law [19]. The measured data coincides with the calculated data well. Hydrogen contents increase with the hydrogen pressure for hydrogen-charging, and HE almost disappears at the hydrogen content of 8.5 mass ppm.

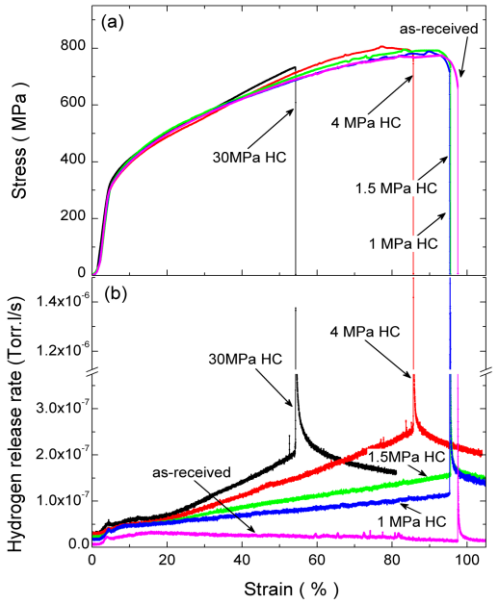

Figure 1. Stress-strain, hydrogen release curves for as-received and hydrogen-charged 304 specimens

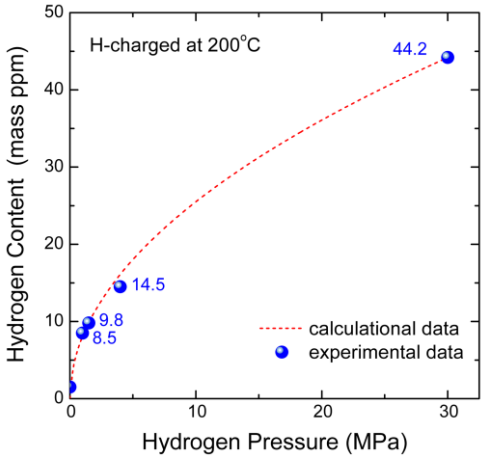

Figure 2. Hydrogen contents of as-received and hydrogen-charged 304 specimens

In order to investigate the dependence of HE on the hydrogen distribution, the hydrogen depth profile is changed by baking. Two 304 specimens were first thermally hydrogen- charged in 30.0 MPa hydrogen gas at 473 K for 250 hours, and then they were baked in vacuum at 433 K for 48 hours. One baked 304 specimen was carried out the DIHR test directly; the other baked specimen was first thinned from the thickness of 1.0 mm to 0.5 mm, and then carried out the DIHR test. Stress-strain, hydrogen release curves for two baked 304 specimens during deformation are shown in Fig. 3. For the hydrogen-charged and baked specimen, the stress-strain curve is similar with those of 1.0 and 1.5 MPa hydrogen-charged and as-received specimens, and HE is almost eliminated. The hydrogen release rate is fairly low and only a sharp peak appears at fracture. For the baked and thinned specimen, it fractures much earlier and shows the obvious HE characteristic. The hydrogen release rate increases with strain after elastic deformation until fracture, as like as the 30.0 MPa hydrogen-charged specimen. Baking at 433 K for 48 hours mainly decreases the hydrogen content in the surface layer and has less effect on the internal hydrogen, while it almost eliminate HE of the 304 specimen. It is clear that hydrogen in the surface layer plays an important role in HE.

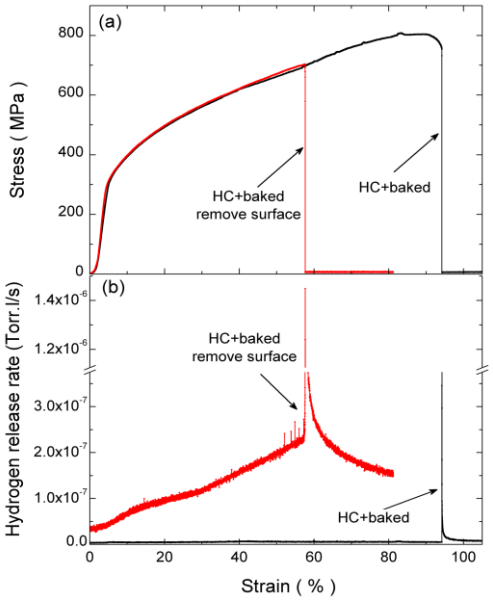

Figure 3. Stress-strain, hydrogen release for curves two baked 304 specimens

The SEM surface topographs of as-received and 30.0 MPa hydrogen-charged 310S and 304 specimens with 40% strain are shown in Fig. 4. For type 310S steel, many slip lines are observed on the surfaces of as-received and hydrogen-charged specimens due to plastic deformation, as shown in Fig. 4(a) and (b), which indicates the obvious characteristic of cross-slip. For type 304 steel, some small holes and white particles are observed on the surface of the hydrogen-charged specimen besides slip lines, as shown in Fig. 4(c) and (d). The small holes are magnified in Fig. 4(e) and the white particles are magnified in Fig. 4(f). The electropolishing has removed the defects and dusts on the specimen surface before the test, thus the white particles must come from the specimen and drop from the small holes. Since the white particles are not observed in the hydrogen-charged 310S specimen and the as-received 304 specimen, these particles may be strain-induced α' martensite broken away from the surface of the hydrogen-charged 304 specimen.

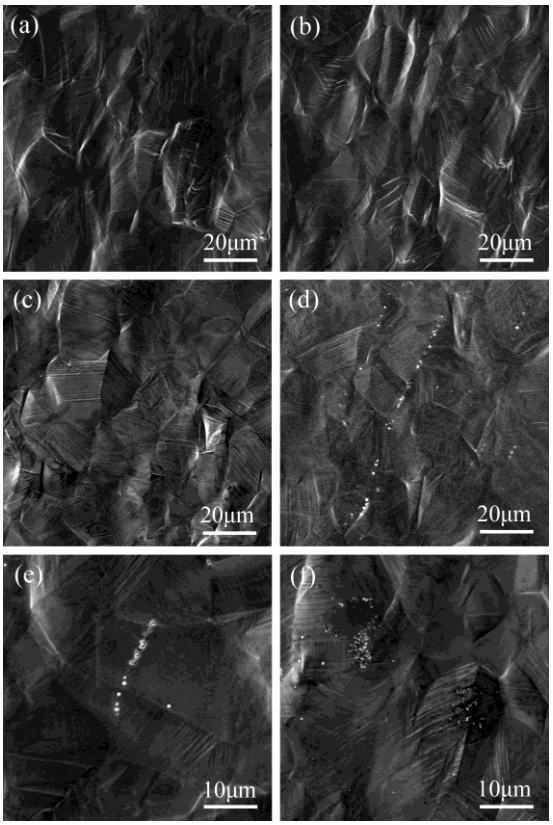

Figure 4. Surface topographs of as-received and hydrogen-charged 310S and 304 specimens with 40% strain. (a) as-received 310S; (b) hydrogen-charged 310S; (c) as-received 304; (d) hydrogen-charged 304; (e) hydrogen-charged 304 with small holes; (f) hydrogen-charged 304 with particles.

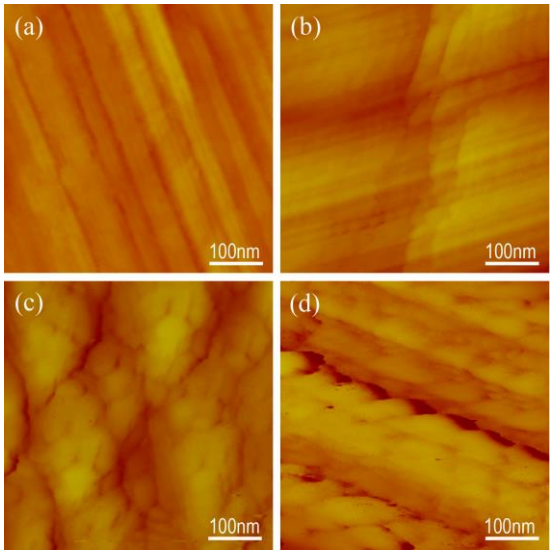

Figure 5. STM images of as-received and hydrogen-charged 310S and 304 specimens with 40% strain. (a) as-received 310S; (b) hydrogen-charged 310S; (c) as-received 304; (d) hydrogen-charged 304.

The STM images of as-received and 30.0 MPa hydrogen-charged 310S and 304 specimens with 40% strain are shown in Fig. 5. For type 310S steel, the slip lines along {111} slip planes are observed on the surfaces of as-received and hydrogen-charged specimens, as shown in Fig. 5(a) and (b). For type 304 steel, the surface rise and fall becomes larger than that of the 310S specimen due to the volume expansion of strain-induced α' martensite, and several small holes along {111} slip planes of austenite (γ) are observed on the surface of the hydrogen-charged 304 specimen, as shown in Fig. 5(c) and (d). The size of the small hole is similar to the size of the white particle in Fig. 4(f), thus HE may cause the particle of α' martensite to break away from the matrix and the small hole is left on the surface. It is obvious that the connection among small holes along {111} slip planes of austenite is liable to form a surface crack.

The SEM fractograph of the 30.0 MPa hydrogen-charged 304 specimen is shown in Fig. 6. It shows a river-like pattern near the surface (indicated by an arrow), which indicates that the crack initiates from the surface and propagates from the surface to interior. For the as-received 304 specimen, the fractograph is completely dimple and the ductile rupture is caused by void coalescence after necking.

4. DISCUSSION

HE of the metal is dependent on hydrogen induced crack initiation and propagation, and the rate of crack propagation is controlled by hydrogen diffusion to accumulate in the triaxial stress region ahead of the crack tip. The origins of hydrogen to HGE and IRHE are different, thus hydrogen induced cracking occurs almost on the surface in HGE, while it generally occurs in the interior in IRHE [10]. However, an early study [11] using SEM showed that the crack initiated at the free surface of hydrogen-charged austenitic steels. Fig. 6 also indicates the crack initiation and propagation from the specimen surface.

The hydrogen content of the hydrogen-charged 304 specimen is 18.1 mass ppm after baking at 433 K for 48 hours. The hydrogen distribution of the baked specimen can be considered diffusion out of a plane sheet (system with constant initial concentration, the surface concentration close to zero in a fairly long period), and the hydrogen depth profile of the baked specimen is calculated from Perng's diffusion coefficient of austenitic steels [20], as shown in Fig. 7. Baking only removes hydrogen in the surface layer, while hydrogen in the interior is still higher. However, baking almost eliminates HE of the hydrogen-charged 304 specimen in spite of the higher hydrogen content inside. When the surface layer with the low hydrogen content has been removed, the new surface layer with the high hydrogen content results in HE again, as shown in Fig. 3. This indicates that it is difficult for hydrogen in the interior to induce the crack, but it is liable for hydrogen in the surface layer to induce the crack from above experimental results.

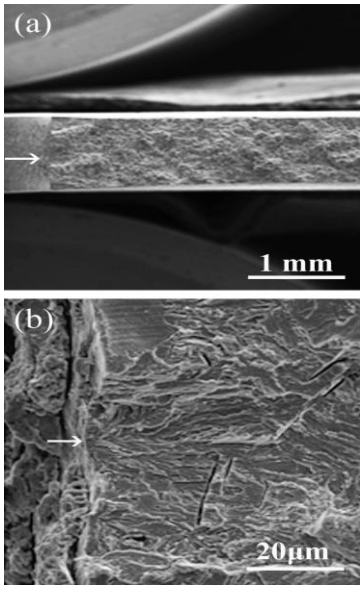

Figure 6. SEM fractograph of the 30.0 MPa hydrogen-charged 304 specimen

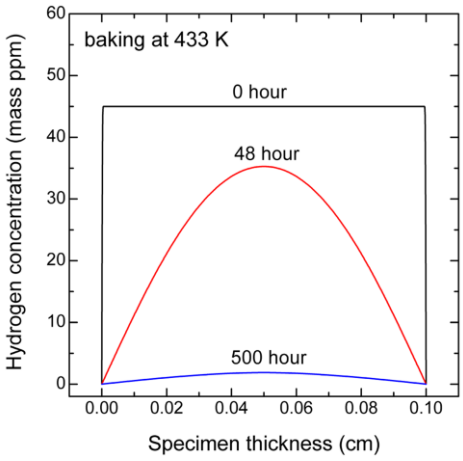

Figure 7. Hydrogen depth profile of the baked specimen

Our previous work shows that HIC initiates and propagates at the boundary between the α'-rich and γ-rich zones in the hydrogen-charged 304 specimen [16], thus HIC will cause the particle of α' martensite formed on the surface to break away from the austenitic matrix and result in some small holes along the slip planes. With increasing strain, these small holes can be connected and form a surface groove. Since the surface is unstable against the nucleation of cracks, it is liable for the crack (or groove) to initiate on the free surface [21]. Therefore, the drop of the α' martensite particles from the matrix may induce crack initiation on the surface of the hydrogen-charged 304 specimen.

Perng and Altstetter [20] reported that the hydrogen diffusivity in α' martensite is several orders of magnitude higher than in austenite, thus α' martensite provides a path for rapid hydrogen transport in metastable austenitic stainless. Our previous result [16] shows that the hydrogen release rate almost remains constant during deformation in hydrogen-charged stable austenitic steels (such as 310S), thus the increase in the hydrogen release rate of the hydrogen-charged 304 specimen during deformation, as shown in Fig. 1, is caused by the α' martensite formation, which is in agreement with Perng's result. The hydrogen content has little effect on the hydrogen release rate during deformation in stable austenitic steels, while it improves the hydrogen release rate of the 304 specimen during deformation due to the α' martensite formation. After baking at 433 K for 48 hours, hydrogen in the interior is still higher, but the hydrogen release rate is fairly low in Fig. 3, which indicates that hydrogen cannot be transported from the interior to surface through α' martensite despite more than 70% α' martensite in the matrix before fracture. Namely, the effect of α' martensite on the long-distance hydrogen transport is weak, and the rapid hydrogen transport of short-circuit caused by α' martensite has not been observed in this study. With increasing strain during deformation, α' martensite forms both in the bulk and near the surface. Since the hydrogen solubility in α' martensite is much lower than that in austenite, the excess hydrogen in α' martensite transformed from austenite near the surface releases from the surface, meanwhile, diffuses to surrounding austenite and accumulates at the α'-γ boundary including numerous defects. For 4.0 and 30.0 MPa hydrogen-charged specimens, hydrogen in the surface layer is enough to induce the surface crack along the α'-γ boundary, and more hydrogen accumulates in the triaxial stress region ahead of the surface crack tip by hydrogen diffusion, which will promote HIC to grow up and propagate, and then cause HE. For 1.0 and 1.5 MPa hydrogen-charged specimens, the α' martensitic transformation increases the hydrogen release rate in Fig. 1, but the hydrogen contents (8.5~9.8 mass ppm) may be not enough to cause the crack propagation before the ultimate tensile strength (UTS). Localized deformation (necking) results in a sudden increase of α' martensite after UTS, and the microstructure with more α' martensite may require less hydrogen for HE, thus the fracture stresses of 1.0 and 1.5 MPa hydrogen-charged specimens increase slightly. For the hydrogen-charged and then baked specimen, although hydrogen in the interior is still high, hydrogen cannot be transported to the surface crack (or groove) from the interior to surface through α' martensite, thus it is difficult for the crack to propagate. From mentioned above, hydrogen in the surface layer plays the primary role in HE due to the difficulty of hydrogen transport from the interior to surface, and this will be favorable to develop the technology for HE prevention in hydrogen utilization.

5. CONCLUSIONS

The hydrogen transport behavior together with HE in hydrogen-charged type 304 stainless steel during deformation was investigated by combined tension and outgassing experiments. The conclusions are as follows:

(1) The hydrogen release rate and HE of hydrogen-charged 304 specimens increase with increasing the hydrogen pressure for hydrogen-charging (or hydrogen content) and almost no HE is observed below the hydrogen content of 8.5 mass ppm.
(2) Baking at 433 K for 48 hours can eliminate HE of the hydrogen-charged 304 specimen, while removing the surface layer will restore HE, which indicates that hydrogen in the surface layer plays the primary role in HE.
(3) Particles attributed to the α' martensite formation break away from the matrix and the small holes form during deformation in the hydrogen-charged 304 specimen. With increasing strain, the connection among small holes along {111} slip planes of austenite will cause crack initiation on the surface, and then HIC propagates from the surface to interior.

ACKNOWLEDGEMENTS

This research is partly supported by the National High Technology Research and Development

Program of China (863 Program, Grant No. 2012AA051504).

REFERENCES

1. Marchi, A.S., Somerday, B.P., Robinson, S.L., Permeability, solubility and diffusivity of hydrogen isotopes in stainless at high gas pressures, Int. J. Hydrogen Energy, **32**, No.1, 2007, pp.100-116.
2. Mine, Y., Narazaki, C., Murakami, K., Matsuoka, S., Murakami, Y., Hydrogen transport in solution-treated and pre-strained austenitic stainless steels and its role in hydrogen- enhanced fatigue crack growth, Int. J. Hydrogen Energy, **34**, No.2, 2009, pp.1097-1107.
3. Michler, T., Naumann, J., Hydrogen environment embrittlement of austenitic stainless steels at low temperatures, Int. J. Hydrogen Energy, **33**, No.8, 2008, pp.2111-2122.
4. Han, G., He, J., Fukuyama, S., Yokogawa, K., Effect of strain-induced martensite on hydrogen environment embrittlement of sensitized austenitic stainless steels at low temperatures, Acta Mater., **46**, No.13, 1998, pp.4559-4570.
5. Zhang, L., Imade, M., An, B., Wen, M., Iijima, T., Fukuyama, S., Yokogawa, K., Internal reversible hydrogen embrittlement of austenitic stainless steels based on type 316 at low temperatures, ISIJ International, **52**, No.2, 2012, pp.240-246.
6. Eliezer, D., Chakrapani, D.G., Altstetter, C.J., Pugh, E.N., The influence of austenite stability on the hydrogen embrittlement and stress-corrosion cracking of stainless steel, Metall. Trans. A, **10A**, No.7, 1979, pp.935-941.
7. Singh, S., Altstetter, C., Effects of hydrogen concentration on slow crack growth in stainless steels, Metall. Trans. A, **13A**, No.10, 1982, pp.1799-1808.
8. Murakami, Y., Kanezaki, T., Mine, Y., Hydrogen effect against hydrogen embrittlement, Metall. Mater. Trans. A, **41A**, No.10, 2010, pp.2548-2562.
9. Zhang, L., Wen, M., Li, Z.Y., Zheng, J.Y., Liu, X.X., Zhao, Y.Z., Zhou, C.L., Materials safety for hydrogen gas embrittlement of metals in high pressure hydrogen storage for fuel cell vehicles, Proceeding of the ASME Pressure Vessels and Piping Conference, 15-19 July 2012, Toronto, 78269.
10. Gray, H.R., Hydrogen embrittlement testing, ASTM STP543, ASTM, 1974, pp.133-151.
11. Buckley, J.R., Hardie, D., The effect of Pre-straining and δ-ferrite on the embrittlement of 304L stainless steel by hydrogen, Corrosion Science, **34**, No.1, 1993, pp.93-107.
12. Repa, P., Oralek, D., Rott, M., Gronych, T., Peksa, L., Stainless steel outgassing due to deformation, Vacuum, **46**, No.8-10, 1995, pp.849-851.
13. Repa, P., Oralek, D., Outgassing stimulated by deformation, Vacuum, **53**, No.1-2, 1999, pp.299-302.
14. Donovan, J.A., Accelerated evolution of hydrogen from metals during plastic deformation, Metall. Trans. A, **7**, No.11, 1976, pp.1677-1683.
15. Shoda, H., Suzuki, H., Takai, K., Hagihara, Y., Hydrogen desorption behavior of pure iron and Inconel 625 during elastic and plastic deformation, Tetsu-to-Hagané, **95**, No.7, 2009, pp.573-580.
16. Zhang, L., An, B., Fukuyama, S., Iijima, T., Yokogawa, K., Characterization of hydrogen- induced crack initiation in metastable austenitic stainless steels during deformation, J. Appl. Phys., **108**, No.10, 2010, 063526.
17. Peressadko, A.G., Nevshupa, R.A., Deulin, E.A., Mechanically stimulated outgassing from ball bearings in vacuum, Vacuum, **64**, No.3-4, 2002, pp.451-456.
18. Zhang, L., An, B., Fukuyama, S., Iijima, T., Yokogawa, K., In-situ characterization of strain localization and strain-induced martensitic transformation in metastable austenitic steels by deformation induced hydrogen and argon releases, J. Appl. Phys., **110**, No.3, 2011, 033540.
19. Sugimoto, H., Fukai, Y., Solubility of hydrogen in metals under high hydrogen pressures: Thermodynamical calculations, Acta Metall. Mater., **40**, No.9, 1992, pp.2327-2336.
20. Perng, T.P., Altstetter, C.J., Effects of deformation on hydrogen permeation in austentic stainless steels, Acta Metall., **34**, No.9, 1986, pp.1771-1781.
21. Yang, W.H., Srolovitz, D.J., Surface morphology evolution in stressed solids: surface diffusion controlled crack initiation, J. Mech. Phys. Solids, **42**, No.10, 1994, pp.1551-1574.